



## **Cassini Orbit Reconstruction From Jupiter to Saturn**

**Duane Roth  
Peter Antreasian  
John Bordi  
Kevin Criddle  
Rodica Ionasescu**

**Robert Jacobson  
Jeremy Jones  
M. Cameron Meek  
Ian Roundhill  
Jason Stauch**

**Guidance, Navigation, and Control Section, Jet Propulsion Laboratory,  
California Institute of Technology, Pasadena, CA 91109**

# **AAS/AIAA Astrodynamics Specialists Conference**

**Lake Tahoe, CA,**

**August 7-11, 2005**

**AAS Publications Office, P.O. Box 28130, San Diego, CA 92198**



## CASSINI ORBIT RECONSTRUCTION FROM JUPITER TO SATURN

**Duane Roth, Peter Antreasian, John Bordi, Kevin Criddle, Rodica Ionasescu,  
Robert Jacobson, Jeremy Jones, M. Cameron Meek, Ian Roundhill, Jason Stauch**

Guidance, Navigation, and Control Section, Jet Propulsion Laboratory,  
California Institute of Technology, Pasadena, CA 91109

After nearly seven years of interplanetary cruise and four planetary gravity assists, the Cassini spacecraft was successfully captured into orbit around Saturn on 1 July 2004. For the first time during the Cassini mission, optical navigation images were obtained and integrated with radio-metric data. Navigators contended with optical navigation images that were potentially biased by Titan's dense atmosphere and Iapetus' albedo variations. Radio-metric data quality was degraded because of small Sun-Earth-probe angles near orbit insertion. The Jupiter to Saturn leg of the spacecraft's trajectory has been reconstructed and is used to provide a metric on navigation performance and maneuver execution errors. In particular, the reconstructed trajectory is compared to trajectory predictions at closest approach to Phoebe, the largest of Saturn's known irregular moons, and at ascending and descending Saturn ring plane crossings. Seven trajectory correction maneuvers, including the Saturn Orbit Insertion burn, are also evaluated and compared to design values.

### INTRODUCTION

After nearly seven years of interplanetary cruise and four planetary gravity assists, Cassini/Huygens was successfully captured into orbit around Saturn on 1 July 2004. The spacecraft's orbit spanning between 7 March 2001 (two months after closest approach to Jupiter) and 17 July 2004 has been reconstructed, completing the set of interplanetary cruise reconstructions from launch to Saturn<sup>1,2,3</sup>. The resulting ephemeris, named 041014R\_SCPSE\_01066\_04199.bsp, has been placed on the Navigation and Ancillary Information File (NAIF) server at <http://naif.jpl.nasa.gov>. Corresponding satellite and planet ephemerides are also included. This paper describes some of the salient features of the reconstructed trajectory. Emphasis is placed on the final few months prior to orbit insertion.

Saturn approach navigation goals were successfully achieved. A 2000 km Phoebe flyby altitude was targeted and, based on the reconstructed trajectory, 2071 km was observed. Relative to predicted three-dimensional control dispersions, the target was missed by only 0.5-sigma. Orbit determination results with a tracking data cutoff five days before the Phoebe flyby (10 days after the targeting maneuver) supported a pointing update and predicted a flyby altitude of 2065 km, encompassing the reconstructed closest approach estimate within a 1.3-sigma error ellipsoid. The close flyby enabled the first direct determination of Phoebe's GM, where an estimated mean value of  $0.5531 \text{ km}^3 \text{ s}^{-2}$  and realistic (as opposed to formal) one-sigma uncertainty of  $0.0010 \text{ km}^3 \text{ s}^{-2}$  was obtained.

The ascending ring plane crossing occurred 4 seconds earlier and 29 km further from the center of Saturn than targeted, equivalent to a 1.1-sigma three-dimensional control error. The descending ring plane crossing, while not targeted, occurred 8 seconds earlier and 114 km closer to the center of Saturn than the

values resulting from the nominal targeting design, resulting in a 1.5-sigma dispersion. The reconstructed trajectory's closest approaches to debris field exclusion zones and rings was  $550\pm 13$  km (Janus/Epimetheus exclusion zone) near the ascending ring plane crossing and  $678\pm 23$  km (Janus/Epimetheus exclusion zone) near the descending ring plane crossing.

## TRACKING DATA

The reconstructed ephemeris was determined from a least squares fit of radio-metric and optical data. Radio-metric data types acquired throughout the span of the reconstructed trajectory were fit. Optical navigation images obtained after 6 February 2004 were fit. Residual plots are presented in Appendix A.

### Radio-Metric Data

X-band range and two-way coherent Doppler data obtained between 28 February 2001 and 13 August 2004 were used in the orbit reconstruction process. Until April 2004, these data were generally acquired at the rate of 3 – 4 passes per week. From the beginning of April until 22 June 2004, the rate of data acquisition was increased to one pass per day. Continuous tracking was implemented from 22 June until after orbit insertion on 1 July 2004. After 2 July, the rate of data acquisition was reduced back to one pass per day. Data acquisition deviated from this schedule near solar oppositions and solar conjunctions. For forty days centered around the 2001 and 2002 solar oppositions and 20 days centered around a month before the 2004 solar opposition, continuous tracking coverage was scheduled in support of the Radio Science Team's gravity wave experiments. Eleven to 25 days of tracking centered around the 2001, 2002, and 2003 solar conjunctions were deleted due to noise and biases induced by solar plasma. Because the 2004 solar conjunction occurred one week after Saturn Orbit Insertion (SOI), a solar corona model was implemented to allow this conjunction data to be included in the fit.

Tracking continuously from 22 June 2004 until 2 July 2004 allowed for the acquisition of three-way coherent Doppler. This data was calibrated for DSN interstation clock offsets and included in the fit so that gaps in tracking coverage occur only between ascending and descending ring plane crossings, when the spacecraft was turned off Earth point. Open loop one-way noncoherent tracking was acquired with the Radio Science Receivers (RSR) while the spacecraft was pointed along the SOI burn attitude. Because of deficiencies in finite burn modeling, attempts to fit this data during SOI execution were unsuccessful. However, 6 minutes of open loop data acquired immediately before SOI and 14 minutes of data acquired immediately after SOI were successfully included in the fit, allowing the SOI burn to be modeled separately from the  $\Delta V$ 's induced by science and ring plane crossing turns.

Doppler weights were applied on a pass by pass basis according to equation 12 in reference 4, where coherent Doppler was compressed to 5 minute intervals and a time constant of 24 hours was assumed. Noncoherent Doppler was compressed to 1 second intervals and a time constant of 1 hour was assumed. A shorter time constant was used for the noncoherent Doppler because only 20 minutes of data is included near Saturn closest approach. Each coherent Doppler pass was therefore weighted by scaling the pass RMS (based on one minute compression) by 3.09. Noncoherent Doppler was weighted by scaling the pass RMS by 7.17.

Range weights were also applied on a pass by pass basis. For this data type, the formal pass uncertainty was scaled by the square root of the number of points within the pass. The intent of this process was to collapse the range information to a single representative point per pass with a weight determined from the standard deviation of the pass. Spacecraft rate information over a pass is then derived primarily from the Doppler data. Ranging parameters were fixed at values resulting in 5 minute cycle times.

Both station to station and pass to pass range biases were estimated. Station to station biases were estimated with an *a priori* uncertainty constraint of 1 meter (1-sigma) and pass to pass biases were estimated with an *a priori* uncertainty constraint of either 3 or 10 meters. The 10 meter constraint was implemented when the spacecraft was within one month of solar conjunction and was derived from an examination of the pass to pass jitter caused by solar plasma during the 2004 conjunction.

## Optical Navigation Data

Optical navigation images (opnavs) of Titan and the icy satellites obtained between 6 February 2004 and 13 August 2004 were used in the orbit reconstruction process. They were scheduled such that the longitudinal coverage for each satellite was approximately evenly distributed. Image phase angles remained relatively constant until orbit insertion, as most images were taken while the spacecraft to Saturn range was much larger than each satellite's orbital radius.

Mimas, Enceladus, Tethys, Dione, and Phoebe opnavs were weighted at 0.05 pixels when the image diameter was less than 3 pixels. Because of its irregular shape and unknown rotation characteristics, Hyperion opnavs were weighted at 0.2 pixels when smaller than 3 pixels. When the image diameter exceeded 3 pixels, weights were computed using a limb track centerfinding algorithm, scaled by a factor determined from examination of post-fit residuals. This algorithm depends on, among other things, the arc length of the lit limb, the pre-fit opnav residual, and pixel DN levels. Rhea weights were computed in this manner exclusively since the earliest Rhea opnav used in the reconstruction had an apparent diameter of 3.6 pixels.

Although even the earliest Titan and Iapetus apparent diameters exceeded 3 pixels, fixed conservative weights were initially favored over the limb track centerfinding algorithm because Titan atmospheric effects and Iapetus albedo variations were capable of skewing the results. These fixed weights were ultimately scaled down after examination of post-fit residuals from a reasonable sized database of Titan and Iapetus observations. Titan opnavs were weighted at 0.2 pixels until 10 June 2004 and Iapetus opnavs were weighted at 0.3 pixels until 13 July 2004. After these respective dates, scaled limb track centerfinding results were implemented.

Star weights were computed by taking the RSS of 0.1 pixel (a minimum reasonable weight) and a value derived from the point spread distribution of pixel DN levels near the star image. Pointing uncertainties about the M (rotation moves picture up/down), N (left/right), and L (rotates picture about its center) axes were estimated from each image with an *a priori* uncertainty constraint of 1 degree per axis.

## PARAMETER ESTIMATION

The orbits of Cassini, the Saturn barycenter, Mimas, Enceladus, Tethys, Dione, Rhea, Titan, Hyperion, Iapetus, and Phoebe were solved for. Planet and satellite *a priori* values and covariance were based on an ephemeris determined from Earth-based and Hubble Space Telescope astrometry combined with observations acquired with the Pioneer 11 and Voyager spacecraft. Correlations between the Saturn barycenter and satellites were maintained.

Besides solving for the epoch states of Cassini, the Saturn barycenter, and satellites, several bias and stochastic parameters were estimated. Dynamic bias parameters included the high gain antenna (HGA) front side diffuse reflectivity, an acceleration induced by spacecraft thermal radiation, a set of solar torque parameters which accounted for reaction control system (RCS) deadband thrusting at various spacecraft sun-relative attitudes, 7 finite burns, 28 impulsive maneuver  $\Delta V$ s, 155 small force  $\Delta V$ s, masses of the Saturn barycenter and satellites (except Hyperion), Saturn's J2, J4, and J6 gravity field coefficients, and the Saturn pole orientation. Nondynamic bias parameters included a one-way Doppler frequency bias, Titan centerfinding biases as a function of phase angle, station to station range biases, and solar corona parameters for the 2004 solar conjunction. Dynamic stochastic parameters included non-gravitational accelerations. Nondynamic stochastic parameters included opnav pointing offsets and pass to pass range biases. Station locations ( $\sim 3$  cm uncertainty), polar motion (2 cm), troposphere calibrations (1 cm wet, 1 cm dry), ionosphere calibrations (1 cm night, 5 cm day), and Hyperion's GM ( $0.35 \text{ km}^3 \text{ s}^{-2}$ ) were considered.

Non-gravitational acceleration models included those from solar pressure, spacecraft thermal radiation, and RCS deadband thrusting. The change in the solar pressure induced acceleration due to estimating the HGA diffuse reflectivity was insignificant. Pre- and post-fit values and uncertainties remained nearly unchanged. The estimate of the spacecraft fixed Z-axis component of the thermally

induced acceleration was refined with tracking data obtained during three gravity wave experiments. During these experiments, the spacecraft Z-axis remained Earth pointed, attitude was maintained with reaction wheels (no thrusting), and continuous radio-metric tracking data was acquired. All gravity wave experiments were performed near solar opposition, where solar plasma effects on tracking data are smallest. The first two experiments were 40 days duration each and the third experiment lasted 20 days. The estimated acceleration at an epoch consistent with SOI was  $-2.85 \times 10^{-12} \text{ km s}^{-2}$  with an uncertainty two orders of magnitude smaller than the mean. Solar torque parameters representing RCS deadband thrusting were not reliably determined since the large *a priori* uncertainty was not substantially reduced.

Impulsive maneuver and small force  $\Delta V$ s were typically modeled with *a priori* uncertainties between 1 and 5  $\text{mm s}^{-1}$ . Spacecraft Y-axis thrusters are coupled, so nearly all  $\Delta V$  is caused by the Z-axis thrusters. Because the HGA boresight is directed along the spacecraft  $-Z$  axis, it is desirable to execute these  $\Delta V$  events while tracking. Many were associated with reaction wheel management, could be directed along the Earth line-of-sight, and were very well determined. Others, such as RCS turns, could not be well determined because the  $\Delta V$  was not directed along the Earth line and, because the HGA could not be directed towards Earth, tracking was unavailable.

The Saturn barycentric system GM *a priori* value and uncertainty was  $37940661 \pm 99 \text{ km}^3 \text{ s}^{-2}$ . The value resulting from the orbit reconstruction was 26 units smaller at  $37940635 \text{ km}^3 \text{ s}^{-2}$  with a one-sigma formal uncertainty of  $16 \text{ km}^3 \text{ s}^{-2}$ . Iapetus' GM was constrained with an *a priori* value and uncertainty of  $127.9 \pm 5.4 \text{ km}^3 \text{ s}^{-2}$ . The post-fit reconstruction value was estimated as  $122.2 \pm 2.2 \text{ km}^3 \text{ s}^{-2}$ . The GM of Phoebe was determined very accurately and is discussed in a later section. Estimates of the other satellite GMs, Saturn's J2, J4, and J6 gravity field coefficients, and the Saturn pole orientation did not differ significantly from the *a priori* information.

Titan phase angle biases were estimated for each Titan image to account for the possibility of systematic observation biases along the sun line as projected into camera coordinates. Phase independent and phase dependent bias terms were estimated, each with *a priori* values of 0 and with relatively unconstrained *a priori* uncertainties of 100% and 10% of Titan's radius respectively.

While tracking data acquired near previous solar conjunctions was not fit, special efforts were implemented to retain the data and improve the orbit accuracy near SOI. The A and B solar corona parameters from reference 5 were estimated in order to reduce range and Doppler biases during the 2004 solar conjunction. A and B partial derivatives were initially computed over the entire data arc. Then, partials associated with tracking data prior to 2004 were zeroed out to prevent a different portion of the solar cycle from degrading the 2004 estimates of A and B. Default *a priori* values and uncertainties of 8000 (A) and 36000 meters (B) were implemented. The A parameter was estimated as  $5216 \pm 1108 \text{ m}$  and B was estimated as  $16061 \pm 7448 \text{ m}$ .

## MANEUVER RECONSTRUCTION

Seven maneuvers are included within the span of the reconstructed trajectory, and parameters from each have been estimated. The third maneuver, TCM-19a, was executed using the monopropellant RCS thrusters. The other six maneuvers were executed using the 440 N main engine bipropellant thruster. Two of the main engine burns, TCM-20 and SOI, were pressurized and the other four were performed in blowdown mode.

TCM-18 and TCM-19 were performed in order to meet a Propulsion Module Subsystem requirement stating that bipropellant maneuvers be no more than 400 days apart. Requiring a minimum duration of 5 seconds, these 'flushing' maneuvers ensure that oxidation of iron alloys in the bipropellant feed system do not plug the small orifices of the valves. TCM-18 was executed on 3 April 2002, 399 days after the previous bipropellant maneuver, and TCM-19 was executed on 1 May 2003, 393 days after TCM-18. Nominal and estimated values and one-sigma uncertainties are presented in Tables 1 and 2, where right ascension and declination are listed in the EME2000 coordinate frame.

Table 1  
TCM-18 NOMINAL AND RECONSTRUCTED VALUES.

	<u>RA(°)</u>	<u>Dec (°)</u>	<u><math>\Delta V</math> (m s<sup>-1</sup>)</u>
Nominal design	195.3±2.3	61.5±1.1	0.901±0.010
Reconstruction	195.8±0.2	61.4±0.2	0.897±0.003

Table 2  
TCM-19 NOMINAL AND RECONSTRUCTED VALUES.

	<u>RA(°)</u>	<u>Dec (°)</u>	<u><math>\Delta V</math> (m s<sup>-1</sup>)</u>
Nominal design	47.0±0.7	21.6±0.7	1.598±0.011
Reconstruction	46.6±0.1	21.7±0.2	1.597±0.003

TCM-19a and TCM-19b were test maneuvers. TCM-19a, designed with a 120 mm s<sup>-1</sup>  $\Delta V$  magnitude in the anti-Earth-line direction and a duration of 3 minutes, exercised a new RCS maneuver block prepared for tour. TCM-19b, designed as a main engine burn with a 2 m s<sup>-1</sup>  $\Delta V$  magnitude and 20 second duration, exercised an Energy-Cutoff Burn algorithm later used during SOI. TCM-19a was executed on 10 September 2003 and TCM-19b was executed less than a month later on 2 October 2003. Nominal and estimated values and one-sigma uncertainties are presented in Tables 3 and 4.

Table 3  
TCM-19a NOMINAL AND RECONSTRUCTED VALUES.

	<u>RA(°)</u>	<u>Dec (°)</u>	<u><math>\Delta V</math> (m s<sup>-1</sup>)</u>
Nominal design	108.0±2.0	22.1±1.8	0.1200±0.0042
Reconstruction	106.8±1.9	21.7±1.8	0.1230±0.0001

Table 4  
TCM-19b NOMINAL AND RECONSTRUCTED VALUES.

	<u>RA(°)</u>	<u>Dec (°)</u>	<u><math>\Delta V</math> (m s<sup>-1</sup>)</u>
Nominal design	29.9±0.5	3.4±0.5	2.000±0.011
Reconstruction	29.8±0.1	3.0±0.1	2.022±0.004

TCM-20's large deterministic  $\Delta V$  targeted to a 2000 km flyby of Phoebe while also aligning the spacecraft trajectory such that the desired Saturn ring plane crossing could be targeted with TCM-21 at small cost. TCM-20 was executed on 27 May 2004, 15 days before closest approach to Phoebe. TCM-20 nominal and estimated values and one-sigma uncertainties are presented in Table 5.

Table 5  
TCM-20 NOMINAL AND RECONSTRUCTED VALUES.

	<u>RA(°)</u>	<u>Dec (°)</u>	<u><math>\Delta V</math> (m s<sup>-1</sup>)</u>
Nominal design	238.776±0.230	28.209±0.203	34.732±0.070
Reconstruction	238.907±0.003	28.227±0.002	34.710±0.002

TCM-21 targeted Cassini to pass 158,500 km from the center of Saturn at the ascending ring plane crossing. At this targeted radius, both ascending and descending ring plane crossings occur between Saturn's F and G rings, where the debris hazard was expected to be minimal. TCM-21 was executed on 16 June 2004, 5 days after the closest approach to Phoebe and 15 days before Saturn periapsis. TCM-21 nominal and estimated values and one-sigma uncertainties are presented in Table 6.

Table 6  
TCM-21 NOMINAL AND RECONSTRUCTED VALUES.

	<u>RA(°)</u>	<u>Dec (°)</u>	<u><math>\Delta V</math> (m s<sup>-1</sup>)</u>
Nominal design	275.28±0.35	-15.44±0.34	3.7048±0.0124
Reconstruction	275.46±0.04	-15.34±0.03	3.6968±0.0005

With a name that describes its purpose, the Saturn Orbit Insertion maneuver was unique in many ways. Timing of this maneuver was critical, as the opportunity to achieve an elliptical orbit around Saturn lasted for only a matter of hours. To increase the probability of performing this maneuver in a timely manner, a second main engine was available to complete the maneuver in the event of an interruption in the prime engine. Yaw steering enhanced this capability by accommodating longer burn interruptions than would have been possible with an inertially fixed burn direction. A pointing bias of  $0.9^\circ$  associated with main engine burns<sup>6</sup> was not corrected in SOI, as operational robustness and simplicity were preferred over the small improvement in targeting accuracy that could have been achieved. To obtain the desired orbit while allowing for burn interruptions, an on-board energy-cutoff burn (ECB) algorithm<sup>7</sup> was implemented. The ECB algorithm used an orbital energy criteria for burn cutoff instead of time or  $\Delta V$ .

SOI was executed on 1 July 2004, starting approximately 25 minutes after the ascending ring plane crossing and ending near Saturn periapsis. Rather than centering the burn around periapsis to minimize  $\Delta V$  cost, this design allowed for science observations closer to Saturn and the inner rings than any time during the tour.

Twenty minutes before turning to the ascending ring plane crossing safe attitude, an antenna swap from the narrow beamwidth HGA to the wider beamwidth LGA was performed and Radio Science Receivers (RSR) successfully acquired the carrier frequency generated by Cassini's Ultra-Stable Oscillator (USO). This resulted in the acquisition of one-way noncoherent Doppler data from approximately 15 minutes before SOI start to (except during ring occultations) about 20 minutes after burn termination. Tracking acquired during pre- and post-SOI spacecraft turns and during the burn itself was discarded because of deficiencies in modeling so that only 6 minutes of data before the burn and 14 minutes of data after the burn could be included in the fit. However, this data enabled a better estimate of SOI by reducing the corrupting effects of two pre-burn turns (to ascending ring plane crossing and SOI burn attitudes) and several post-burn turns (to science observation attitudes, descending ring plane crossing attitude, and Earth-point). Examination of the Radio Science residuals also enabled a precise determination of the burn start and end times. The burn was then modeled by specifying a start time and duration to be consistent with values derived from residuals. To maintain a fixed burn duration while allowing the  $\Delta V$  to vary, thruster force was estimated instead of  $\Delta V$ . SOI nominal and estimated values and one-sigma uncertainties are presented in Table 7.

Table 7  
SOI NOMINAL AND RECONSTRUCTED VALUES.

	<b>RA(<math>^\circ</math>), <u>RA rate (<math>^\circ \text{ s}^{-1}</math>)</u></b>	<b>Dec (<math>^\circ</math>), <u>Dec rate (<math>^\circ \text{ s}^{-1}</math>)</u></b>	<b>Thrust (N), <u>Thrust rate (<math>\text{N s}^{-1}</math>)</u></b>
Nominal design	-111.096 $\pm$ 0.201, (7769 $\pm$ 777) $\times 10^{-6}$	0.029 $\pm$ 0.201, (1768 $\pm$ 177) $\times 10^{-6}$	437.00 $\pm$ 7.28, (0 $\pm$ 100) $\times 10^{-5}$
Reconstruction	-111.030 $\pm$ 0.004, (7733 $\pm$ 2) $\times 10^{-6}$	0.056 $\pm$ 0.006, (1739 $\pm$ 2) $\times 10^{-6}$	441.11 $\pm$ 0.05, (68 $\pm$ 2) $\times 10^{-5}$

Right ascension and declination rate terms were estimated to account for yaw steering deviations from the nominal profile. The estimation of fourth order thrust polynomials was initially investigated before finally settling on the first order model given in Table 7, as higher order models did not reduce Doppler residuals acquired during the burn. With these estimated values, the reconstructed SOI model leads to a  $\Delta V$  of 626.8  $\text{m s}^{-1}$ , a duration of 5780.5 seconds, and a mass decrement of 841.5 kg. The average thruster force during the burn is derived as 443.1 N. Corrections to SOI estimated values were sub-sigma, allowing the SOI cleanup maneuver, scheduled three days after SOI, to be cancelled.

## PHOEBE FLYBY

A close flyby of Phoebe, the largest of Saturn's known irregular moons, was a key objective of the Cassini mission. Because Phoebe's orbital radius is nearly 4 million kilometers greater than Cassini's maximum orbital radius after capture into orbit, the only opportunity to achieve this objective was prior to Saturn orbit insertion. TCM-20 targeted the Cassini spacecraft to an altitude 2000 km from Phoebe and was

executed on 27 May 2004. It resulted in a 2071 km closest approach to Phoebe fifteen days later at 11 June 19:34 UTC.

The flyby has yielded the first direct determination of Phoebe’s GM. A mean value of  $0.5531 \text{ km}^3 \text{ s}^{-2}$  with a formal one-sigma uncertainty of  $0.0004 \text{ km}^3 \text{ s}^{-2}$  was obtained from the reconstruction, but based on sensitivities to data weights and non-gravitational accelerations, the formal uncertainty has been scaled up to a more realistic value of  $0.0010 \text{ km}^3 \text{ s}^{-2}$ . Using the gravitational constant  $G = (6.6742 \pm 0.0010) \times 10^{-23} \text{ km}^3 \text{ g}^{-1} \text{ s}^{-2}$  (reference 8), the mass of Phoebe is estimated to be  $(8.287 \pm 0.015) \times 10^{21} \text{ g}$ .

Targeted and estimated values are presented in Figure 1, where B-plane coordinate system axes (Appendix B) are centered at Phoebe and the T-axis is directed parallel to the Earth Mean Orbital Plane at the J2000 epoch. One-sigma control dispersions resulting from orbit determination uncertainties and TCM-20 execution errors are included with target values. To reduce the effect of control dispersions on science observations, pointing updates based on a late orbit determination estimate were necessary. A ‘Live Update OD’, with a data cutoff five days before Phoebe closest approach, reduced orbit uncertainties considerably, satisfying one-sigma pointing requirements of  $0.79^\circ$  and  $1.02^\circ$  per axis for ranges greater than 30,000 and 20,000 km respectively. Target, estimates, and dispersions from Figure 1 are tabulated in Table 8.

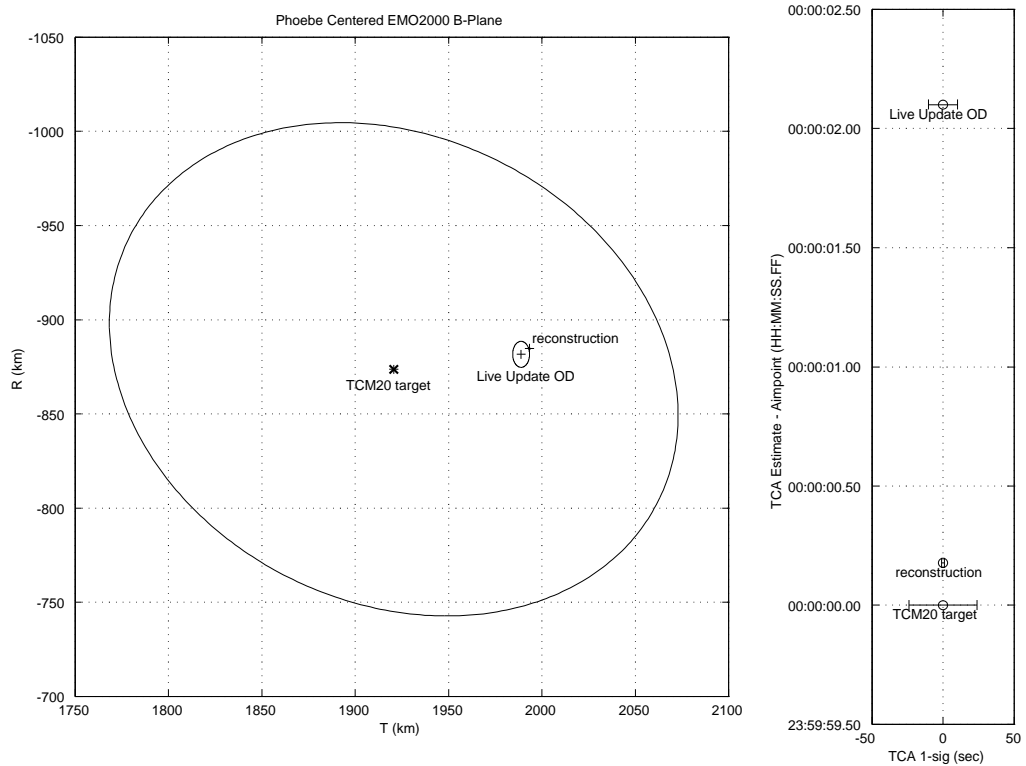


Figure 1. Phoebe B-plane Target and Solutions.

Table 8  
PHOEBE FLYBY NOMINAL AND ESTIMATED VALUES.

	<b><u>B.R (km)</u></b>	<b><u>B.T (km)</u></b>	<b><u>Closest Approach Time (UTC)</u></b>
TCM-20 Target	-874±131	1921±152	11 June 2004 19:33:37±24 s
Live Update OD	-881.65±6.91	1988.84±4.52	11 June 2004 19:33:39±10 s
Reconstruction	-884.70±0.34	1993.36±0.34	11 June 2004 19:33:37.2±1.0 s

From the Phoebe targeting maneuver on 27 May until the next maneuver on 16 June 2004, range and two-way coherent Doppler data were acquired at the rate of approximately six hours per day. An outage of approximately 35 hours, 20 minutes centered near closest approach resulted when the spacecraft high gain antenna was turned away from Earth so that science instruments could be pointed toward Phoebe. Two of the optical navigation images taken each day from 27 May to 8 June were of Phoebe. The navigation team also used ninety-six of the Phoebe science images taken on 11 and 12 June.

Cassini’s attitude was maintained with reaction wheels from 27 May to 16 June. Thrusters were fired to reduce reaction wheel momentum only once, on 5 June. The resulting  $0.5 \text{ mm s}^{-1} \Delta V$  was directed along the Cassini-Earth line during a tracking pass and was determined to an accuracy well within  $0.1 \text{ mm s}^{-1}$ . Spacecraft-fixed, thermally induced mean accelerations were accounted for by implementing an attitude model based on AACS’ c-kernels (files containing time history of spacecraft orientation) after 22 December 2003. File size limitations prevented use of c-kernels prior to this date. Thermally induced acceleration uncertainties were approximately  $0.2 \times 10^{-12} \text{ km s}^{-2}$ . Solar pressure induced accelerations were approximately  $0.5 \times 10^{-12} \text{ km s}^{-2}$  at this heliocentric range and were accounted for with stochastic estimates around a mean model with a 20% uncertainty. Estimates were updated every eight hours and were assumed to be uncorrelated.

### RING PLANE CROSSING

Following the successful flyby of Phoebe, Cassini’s trajectory was targeted to minimize the possibility of debris impact near the ring plane while holding the SOI maneuver design fixed. TCM-21 accomplished this goal by targeting the ascending ring plane crossing to a radius of 158,500 km from the center of Saturn. The resulting trajectory passes between Saturn’s F and G rings while avoiding putative debris fields near the orbits of Janus, Epimetheus, and Mimas. Figures 2 and 3 show the trajectory at ascending and descending node crossings and provides closest approach distances to the F ring, G ring, and debris fields. Three-sigma boundaries for each of the exclusion zones are provided in Table 9.

Table 9  
THREE-SIGMA EXCLUSION ZONE BOUNDARIES.

	<b>Inner radius (km)</b>	<b>Outer radius (km)</b>	<b>Height above equator plane (km)</b>	<b>Height below equator plane (km)</b>
F ring	140,180	140,270	20	20
J/E exclusion zone	149,775	153,054	1064	1061
G ring	165,000	176,000	720	720
Mimas debris field	181,772	189,268	4953	4953

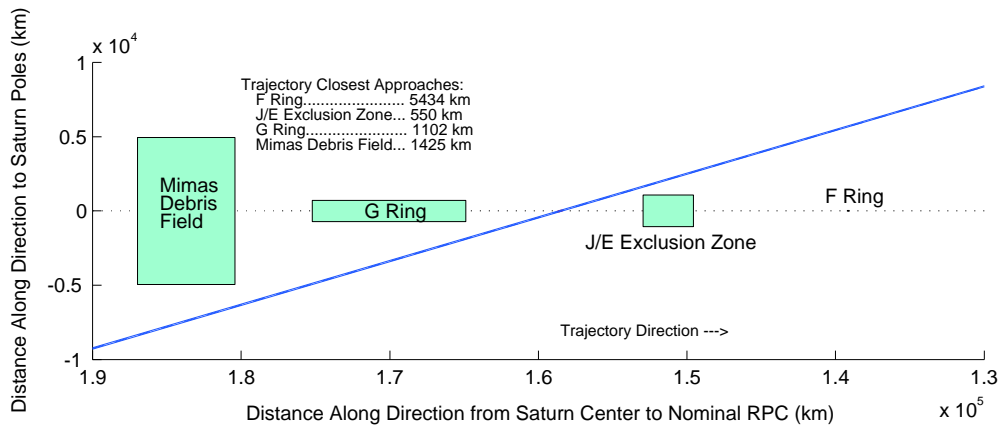


Figure 2. Ascending Node Trajectory.

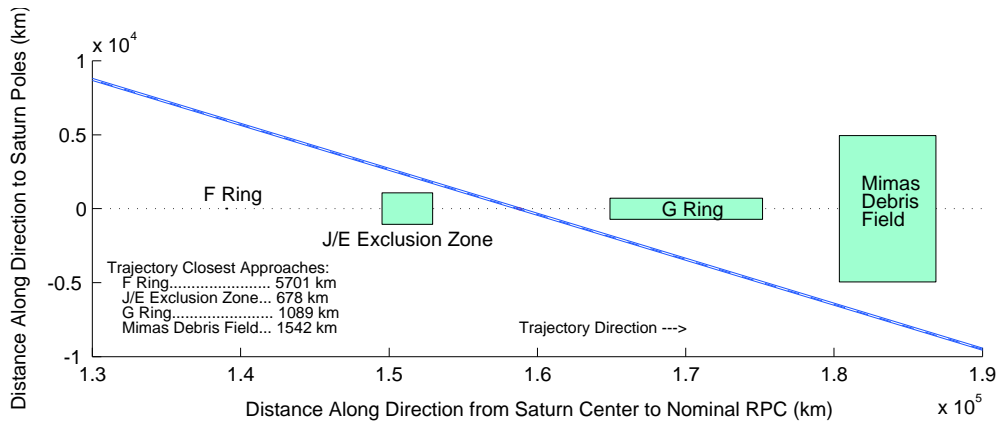


Figure 3. Descending Node Trajectory.

TCM-21 target and control accuracy are compared to the reconstructed ascending ring plane crossing in Table 10 and Figure 4. Coordinates are listed in the inertial Saturn true equator of date frame and uncertainties are 1-sigma. Here, the target has been converted from a radius of 158500 km, right ascension of 157.8°, and declination of 0.0° to Cartesian coordinates.

Table 10  
COMPARISON OF TARGETED AND ACHIEVED ASCENDING RING PLANE CROSSING.

	<u>X (km)</u>	<u>Y (km)</u>	<u>Radius (km)</u>	<u>Date/time (ET)</u>
Target	-146750.5±28.2	59887.8±53.9	158500±45.1	1 Jul 2004 00:47:38± 4.91 s
Reconstruction	-146772.6±0.2	59909.6±0.5	158528.7±0.4	1 Jul 2004 00:47:34.10±0.02 s

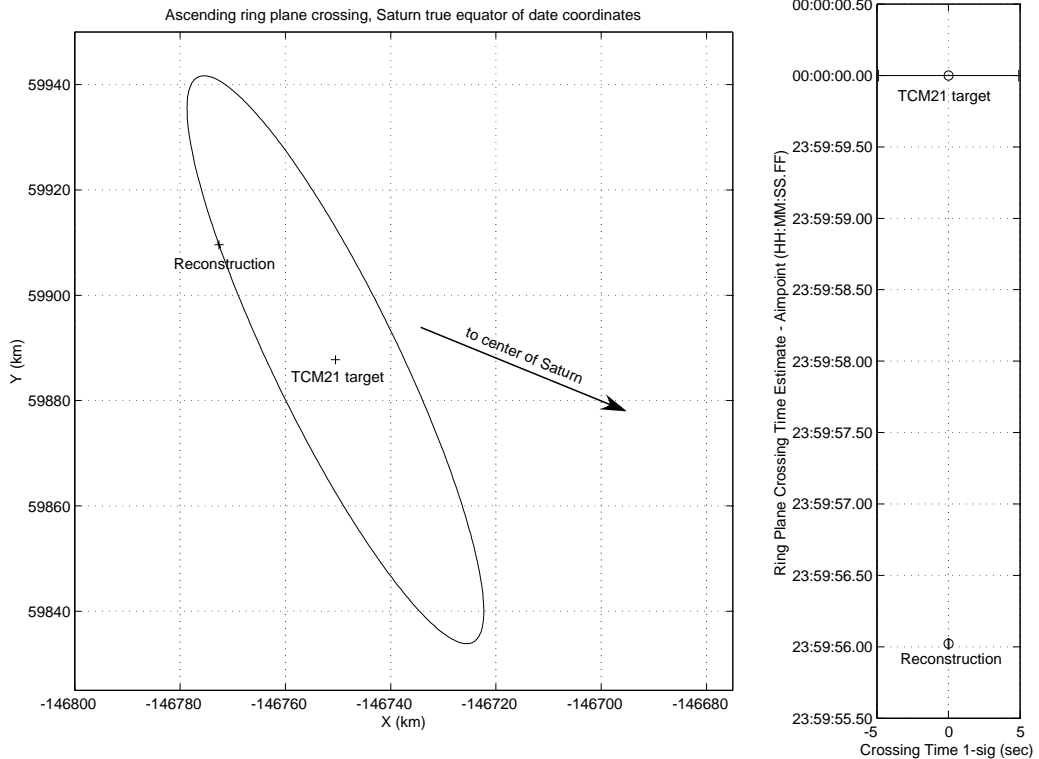


Figure 4. Targeted and Achieved Ascending Ring Plane Crossing.

Cassini was not targeted to the descending ring plane crossing, as this would have involved an undesirable late update to the SOI maneuver design. However, the descending ring plane crossing was monitored closely in operations to ensure that Cassini's trajectory remained a safe distance from exclusion zones. Table 11 and Figure 5 compare the nominal descending ring plane crossing with the reconstructed values, where the nominal value is taken from the TCM-21 final design with an updated SOI model accounting for the intentionally uncorrected 0.9° thrust vector pointing offset.

Table 11  
COMPARISON OF NOMINAL AND ACHIEVED DESCENDING RING PLANE CROSSING.

	<u>X (km)</u>	<u>Y (km)</u>	<u>Radius (km)</u>	<u>Date/time (ET)</u>
Nominal	146189.9±82.7	-62246.9±36.3	158890.4±79.6	1 Jul 2004 04:35:02.84± 5.97 s
Reconstruction	146075.8±0.4	-62223.9±0.2	158776.4±0.3	1 Jul 2004 04:34:55.12±0.02 s

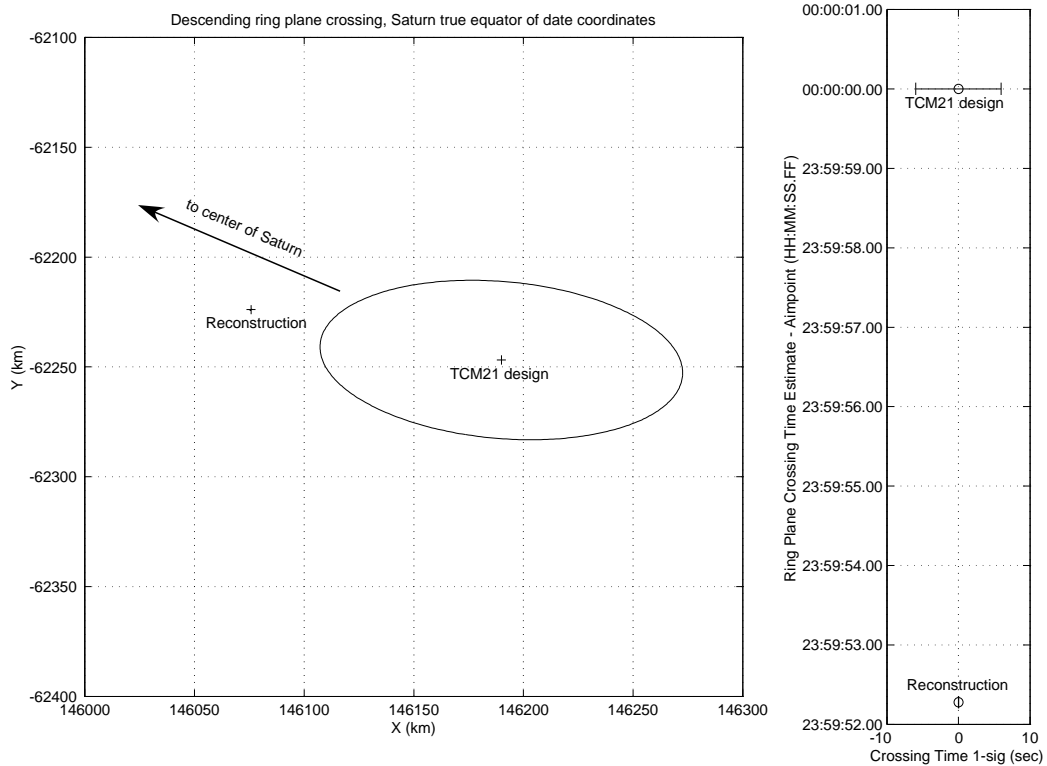


Figure 5. Nominal and Achieved Descending Ring Plane Crossing.

## POSITION UNCERTAINTIES

Spacecraft and satellite ephemeris uncertainties associated with the approach trajectory reconstruction are provided in Appendix C. This appendix provides plots of formal one-sigma position uncertainties as a function of time for Cassini and Saturn's major satellites relative to the Saturn system barycenter. Coordinates are aligned along the body velocity direction, angular momentum direction, and, to complete the orthogonal system, along the direction defined by the cross product of velocity and angular momentum directions. Uncertainties are provided from 12 March 2004, when the spacecraft enters the Saturn sphere of influence, until 17 July 2004, when the reconstructed ephemerides end.

## CONCLUSIONS

Saturn approach navigation goals were successfully achieved. Goals included meeting pointing requirements during the Phoebe flyby, avoiding the debris exclusion zones near ascending and descending ring plane crossings, and capture into orbit about Saturn. Execution errors associated with TCM-18 through SOI were nearly all sub-sigma, with TCM-19b's two-sigma  $\Delta V$  errors being the only exception. The reconstructed trajectory passes 0.5-sigma from the Phoebe flyby target and 1.3-sigma from the Phoebe knowledge update based on three-dimensional control and Live update OD dispersions. The reconstructed ascending node ring plane crossing deviated from the targeted value by 1.1-sigma, while for the descending node, the crossing deviated from the TCM21 design value by 1.5-sigma. Debris exclusion zone closest approaches were  $550 \pm 13$  km near the ascending node and  $678 \pm 23$  km near the descending node.

## ACKNOWLEDGEMENTS

Ninety-six Phoebe science images provided by Carolyn Porco and the rest of the Imaging Science Subsystem were used in this analysis to improve the accuracy of Cassini's orbit relative to Phoebe. All of these images were captured near closest approach to Phoebe, on 11 and 12 June 2004.

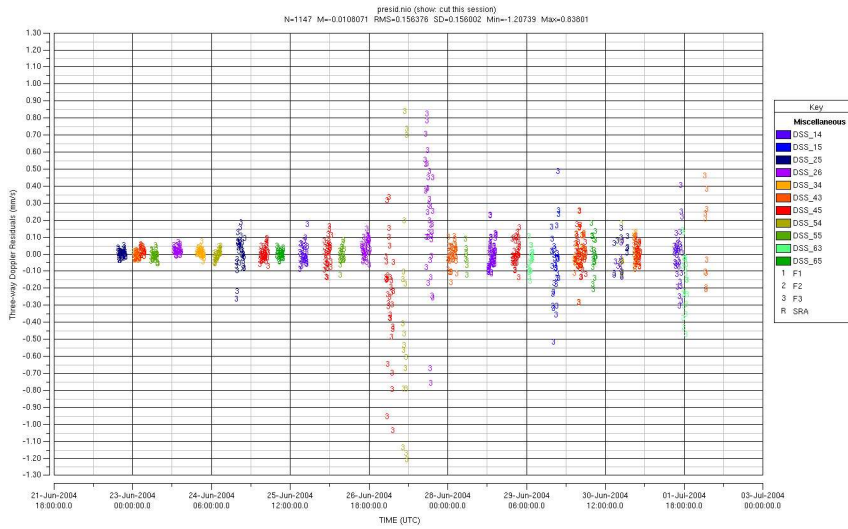
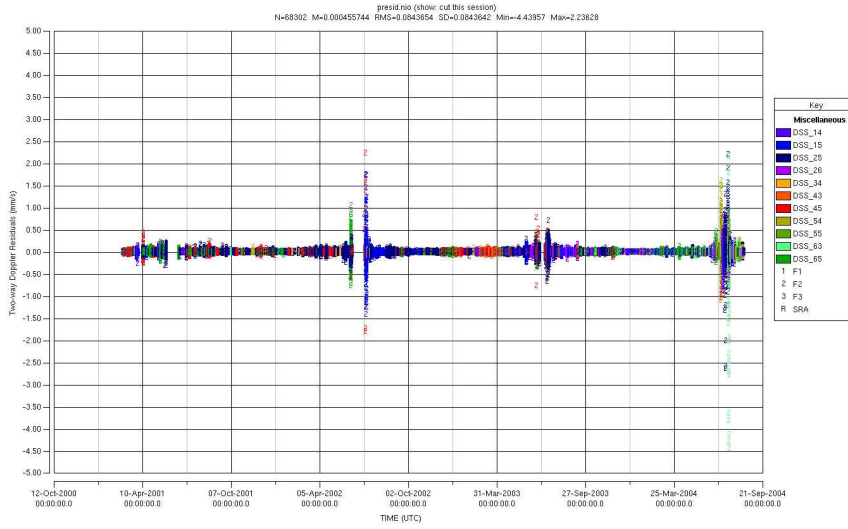
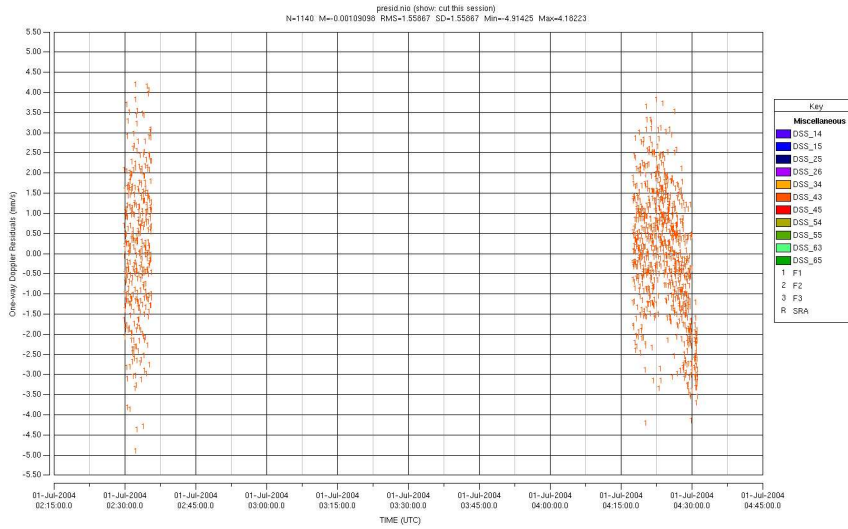
Approximately two hours of noncoherent Doppler tracking data provided by Sami Asmar and the Radio Science Systems Group were used to improve SOI burn modeling. Data were acquired via Radio Science Receivers from 15 minutes before SOI start to 20 minutes after burn termination (with some outages during ring occultations). Extensive analysis and pre-processing was performed by RSSG member Doug Johnston.

This research was carried out at the Jet Propulsion Laboratory, California Institute of Technology, under a contract with the National Aeronautics and Space Administration. Reference to any specific commercial product, process, or service by trade name, trademark, manufacturer or otherwise, does not constitute or imply its endorsement by the United States Government or the Jet Propulsion Laboratory, California Institute of Technology.

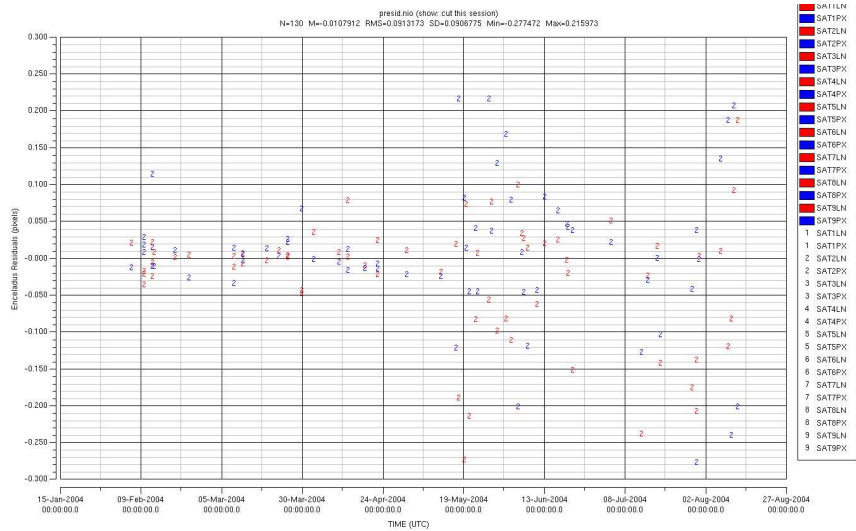
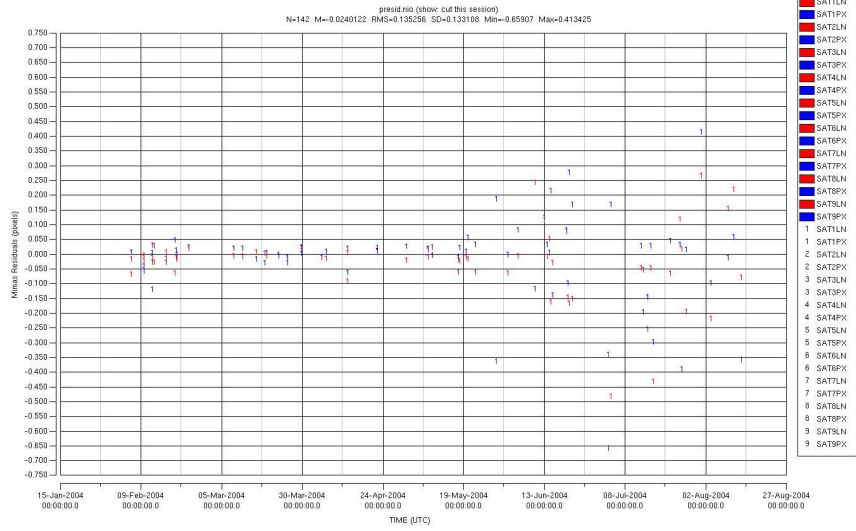
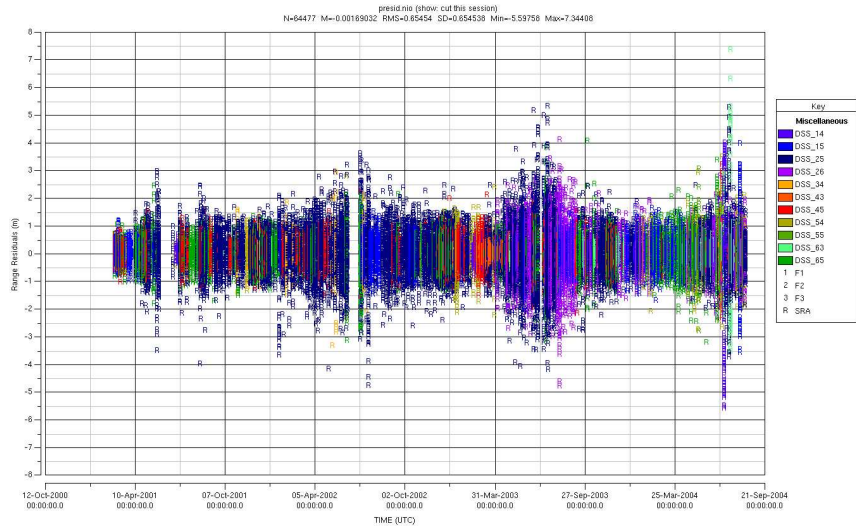
## REFERENCES

1. Roth, D. C., Guman, M. D., Ionasescu, R., and Taylor, A. H., "Cassini Orbit Determination From Launch to the First Venus Flyby,,," Paper AIAA-98-4563, AIAA/AAS Astrodynamics Specialist Conference, Boston, Massachusetts, August 1998.
2. Guman, M. D., Roth, D. C., Ionasescu, R., Goodson, T. D., Taylor, A. H., Jones, J. B., "Cassini Orbit Determination From First Venus Flyby to Earth Flyby,,," Paper AAS 00-168, AAS/AIAA Space Flight Mechanics Meeting, Clearwater, Florida, January 2000.
3. Roth, D. C., Guman, M. D., Ionasescu, R., "Cassini Orbit Reconstruction From Earth to Jupiter,,," Paper AAS 02-156, AAS/AIAA Space Flight Mechanics Meeting, San Antonio, Texas, January 2002.
4. Folkner, W. M., "Effect of uncalibrated charged particles on Doppler tracking,,," IOM 335.1-94-005, 1 March 1994.
5. Moyer, T. D., "Formulation for Observed and Computed Values of Deep Space Network Data Types for Navigation,,," Section 10, JPL Publication 00-7, October 2000.
6. Goodson, T. D., Gray, D. L., Hahn, Y., and Peralta, F., "Cassini Maneuver Experience: Finishing Inner Cruise,,," Paper AAS 00-167, AAS/AIAA Astrodynamics Specialist Conference, Clearwater, Florida, January 2000.
7. Goodson, T. D., "Evaluation of an Energy-Cutoff Algorithm for the Saturn Orbit Insertion Burn of the Cassini-Huygens Mission,,," Paper AAS 04-133, AAS/AIAA Astrodynamics Specialist Conference, Maui, Hawaii, February 2004.
8. Mohr, P.J., Taylor, B.N., "The 2002 CODATA Recommended Values of the Fundamental Physical Constants,,," (Web Version 4.2), <http://physics.nist.gov/cuu/Constants/index.html>, National Institute of Standards and Technology, Gaithersburg, MD 20899.

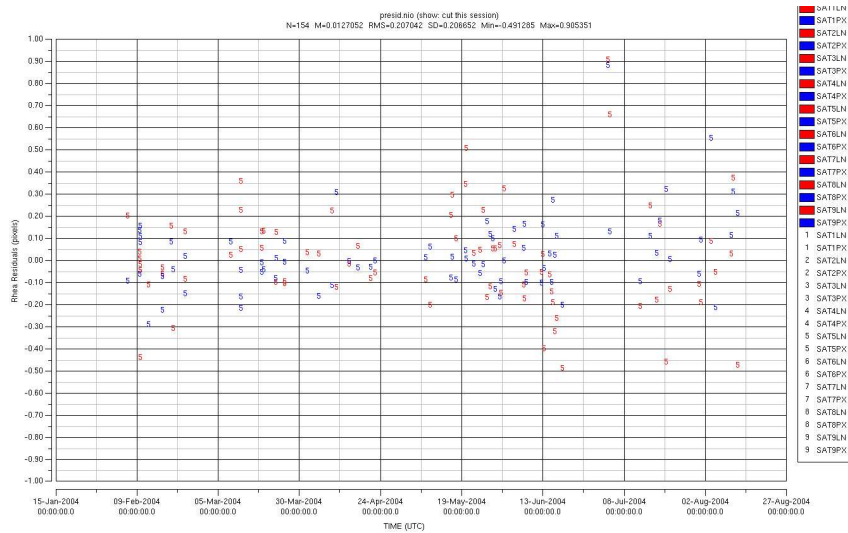
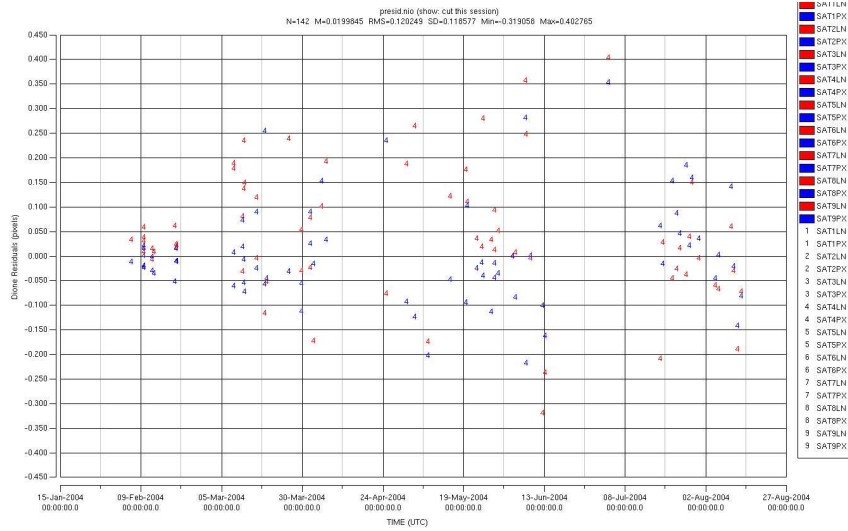
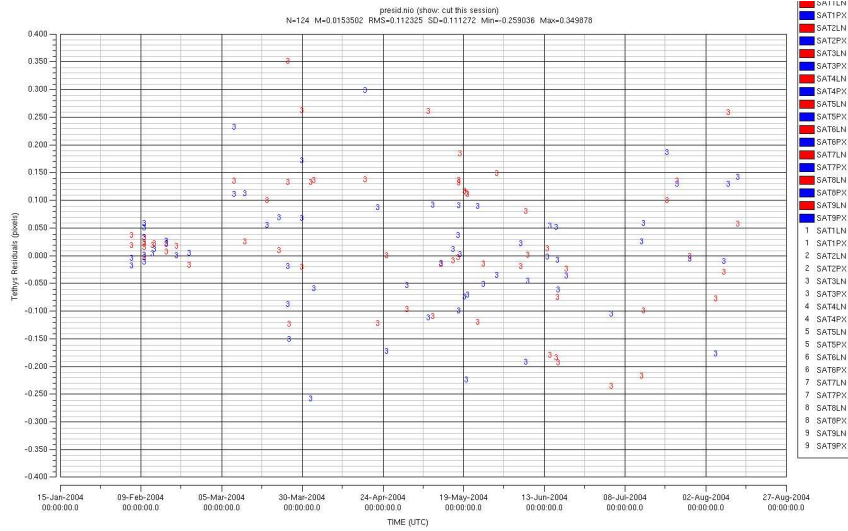
# APPENDIX A - Data Residuals



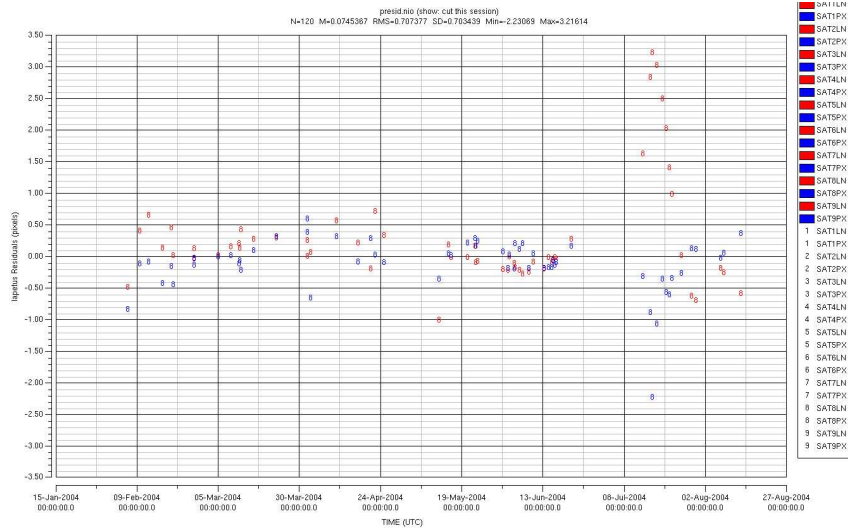
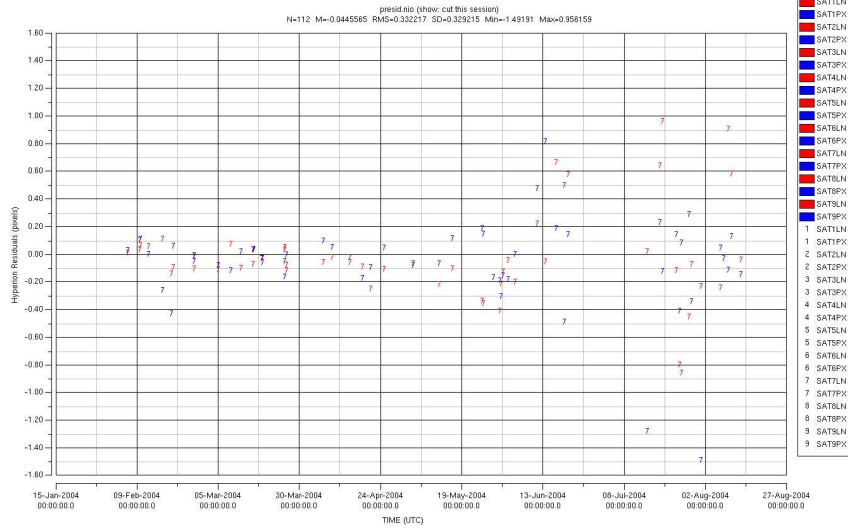
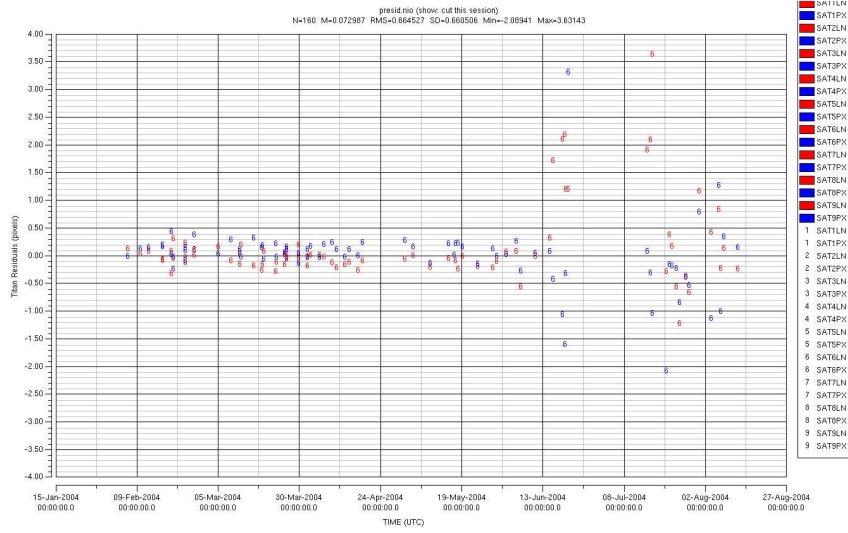
## APPENDIX A - Data Residuals (continued)



# APPENDIX A - Data Residuals (continued)



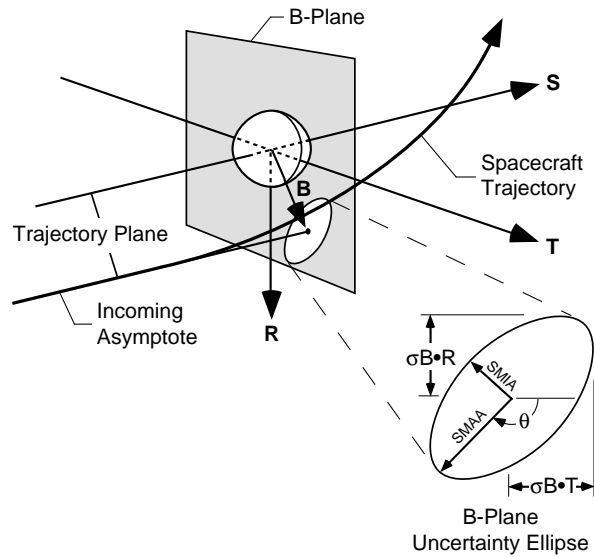
## APPENDIX A - Data Residuals (continued)



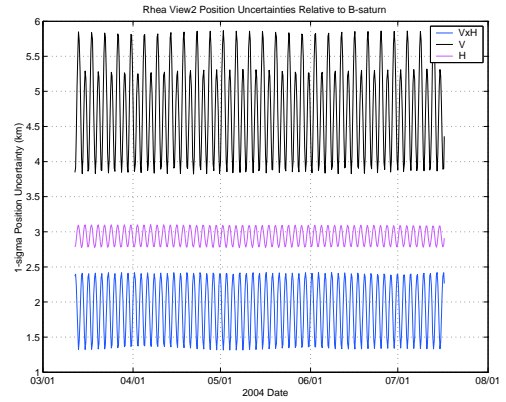
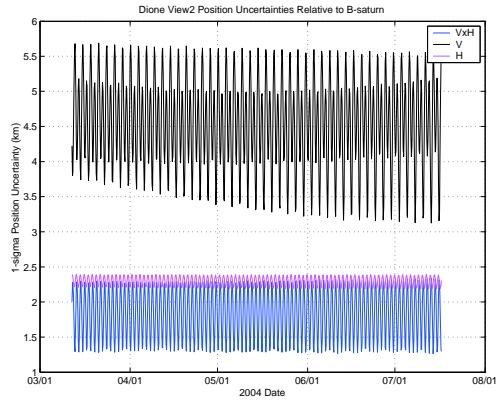
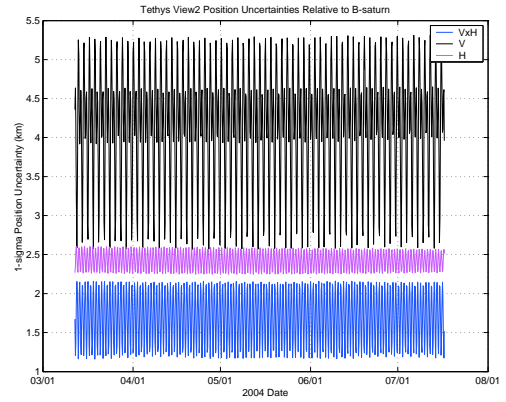
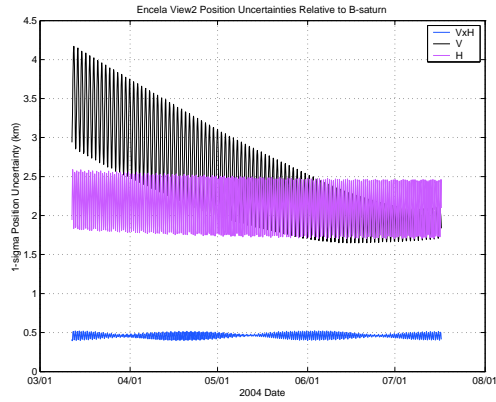
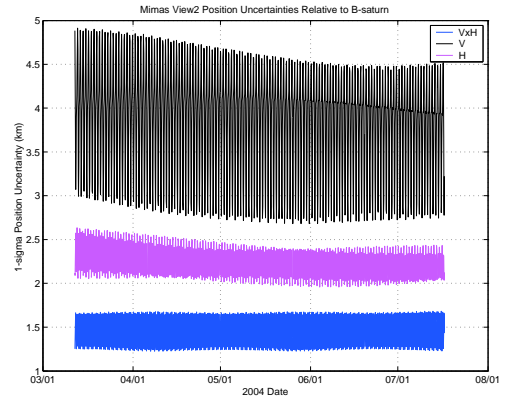
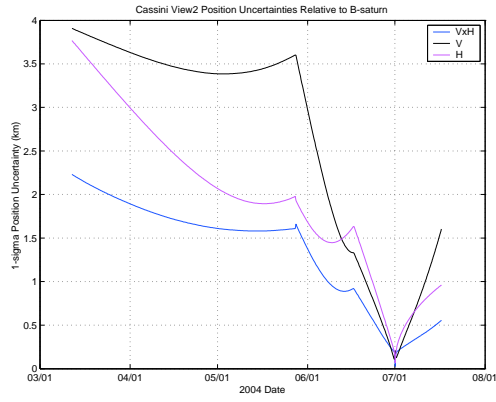


## APPENDIX B – B-plane Description

The B-plane passes through the center of the target body and perpendicular to the incoming asymptote of the hyperbolic flyby trajectory. Coordinates in the plane are given in the **R** and **T** directions, with **T** being parallel to the Earth Mean Orbital plane of 2000 (in the direction defined by crossing **S** into the pole vector). The angle  $\theta$  determines the rotation of the semi-major axis of the error ellipse in the B-plane relative to the T-axis and is measured positive right-handed about **S**.



# APPENDIX C – One-sigma Reconstructed Position Uncertainties



## APPENDIX C – One-sigma Reconstructed Position Uncertainties (continued)

